# Quantum kinetic theory of two-beam current injection in bulk semiconductors

P. Král and J. E. Sipe
*Department of Physics, University of Toronto, 60 St. George Street, Ontario, Toronto M5S 1A7, Canada*
(Received 11 March 1999; revised manuscript received 1 September 1999)

We develop a theory of current injection in bulk semiconductors by simultaneous excitation with two laser beams with frequencies $2\omega_0$, $\omega_0$. Coherent mixing of the resulting one- and two-photon transitions generates an *effective field* $A_{eff}(\mathbf{k})$ with different strengths at $\pm\mathbf{k}$ points in momentum space. This asymmetry in carrier generation, producing the induced current, is *controlled* by the relative phase of the two fields. Quantum kinetic equations for the photogenerated carriers are derived from nonequilibrium Green functions. They are simplified here to the Boltzmann limit, and applied to a model of GaAs in the presence of LO phonons. Different forms of the conduction electron distributions result for generation from light- and heavy-hole bands, and give different saturation and relaxation rates for the induced current. Generation of THz radiation by the current is also discussed.

## I. INTRODUCTION

Two coherent laser beams at frequencies $2\omega_0$ and $\omega_0$, connecting the ground state of an atom to its ionized states by one- and two-photon transitions, respectively, can be used to eject electrons in a preferred direction by adjusting the relative phase of the two beams.[1] The effect is a consequence of a *quantum interference* between electron wave function components of different parities, associated with the two transition processes. An analogous scheme has been suggested for the control of the ionization of a defect in a semiconductor,[2] and later such an injection of dc current was observed in a semiconductor quantum well.[3]

More recently, it has been realized that two-beam injection of dc current can be effected by excitation of a bulk semiconductor above the gap,[4] where the band-gap energy $E_g$ satisfies $2\hbar\omega_0 > E_g > \hbar\omega_0$. Here the current injection in conduction and valence bands follows naturally from the fact that one- and two-photon excitation amplitudes interfere differently for wave vectors $\mathbf{k}$ and $-\mathbf{k}$. The injection rates have been calculated using a Fermi's golden rule approach for typical semiconductors, with the momentum relaxation described by the inclusion of a phenomenological relaxation time in the hydrodynamic equations for the current.[4] This gives a semiquantitative agreement between theory and experiment,[5,6] but the kinetics of carrier injection and relaxation has not yet been studied. Other current injection schemes[7] and coherent control methods have been also investigated.[8–10]

We use nonequilibrium Green functions[11–16] to derive quantum kinetic equations for the two-beam current injection and relaxation. From a diagrammatic analysis we first find an effective *field self-energy* $\Sigma_f$, describing the quantum interference of the one- and two-photon processes, and giving a tunable anisotropy of injected carrier population in the Brillouin zone. The absolute value of $\Sigma_f$ forms the *expansion parameter* in the transport equations. We explicitly find quantum kinetic equations quadratic in $\Sigma_f$. For our model calculations, they are simplified to the Boltzmann limit and solved for pulsed and steady-state excitations in bulk GaAs, in the presence of scattering by LO phonons. The injection of carriers from light (lh) and heavy hole (hh) bands gives different electron distributions in the conduction band and different momentum relaxation rates.[17]

The paper is organized as follows. In Sec. II we present the model for the photogeneration and relaxation of carriers in bulk semiconductors. In Sec. III the field self-energy $\Sigma_f$ for two-beam injection is obtained. Section IV is devoted to the derivation of the approximated quantum kinetic equations. Numerical results of the current injection in GaAs, in the Boltzmann approximation, are presented in Sec. V.

## II. MODEL SYSTEM

In Fig. 1 we schematically show the excitation of a semiconductor by two laser beams. The fields, with frequencies $2\omega_0$ and $\omega_0$, lead to one- and two-photon transitions between the valence and conduction bands, respectively. The transition amplitudes for the two processes have opposite parities in reciprocal space, so their interference can result in differ-

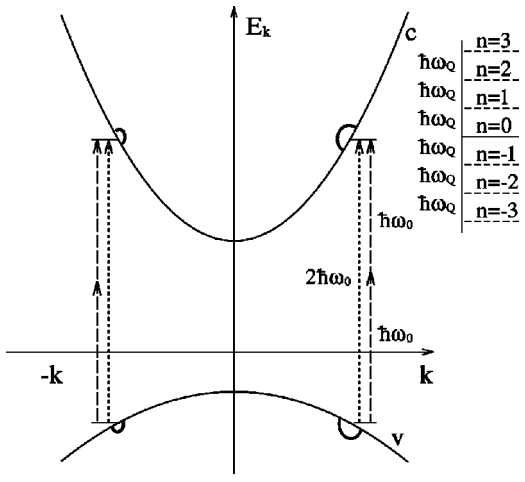


FIG. 1. Excitation of the semiconductor at $\pm\mathbf{k}$ mixing transition amplitudes from the two optical fields. The following carrier relaxation by LO-phonon emissions, and absorptions are denoted by formal levels with the index *n*.

 

ent carrier generation rates at $\pm\mathbf{k}$ in the Brillouin zone. In coherent control experiments,[5,6] injected currents can be observed with injected carrier densities as low as $n_i \approx 10^{14}$ cm$^{-3}$. At such low densities, scattering from LO phonons, indicated in Fig. 1, provides the fastest relaxation of the momentum of excited particles.

Even at these low densities, carrier-carrier interactions[18] can modify the current injection through excitonic effects.[19] These become negligible far above the band gap, and for simplicity we neglect them here. At larger injection densities, $n_i \approx 10^{16}$ cm$^{-3}$, carrier-carrier scattering dominates over LO-phonon scattering.[20,21] Then the injected carrier populations, with opposite quasimomenta in the conduction and valence bands, can rapidly thermalize to form hot Fermi seas, with their center wave vectors shifted from the center of the Brillouin zone. At higher densities, momentum relaxation by Auger transitions between the conduction and valence bands can also become important.[22]

Here we only consider current injection in the low carrier density limit, and model our system by a Hamiltonian that includes only LO-phonon scattering:

$$H=\sum_{\alpha;\mathbf{k}} \varepsilon_\alpha(\mathbf{k}) a^\dagger_{\alpha,\mathbf{k}} a_{\alpha,\mathbf{k}} - \sum_{\alpha,\beta;\mathbf{k}} \frac{e}{c}\mathbf{A}(t) \cdot[\mathbf{v}_{\alpha\beta}(\mathbf{k}) a^\dagger_{\alpha,\mathbf{k}} a_{\beta,\mathbf{k}} + \text{H.c.}] + \sum_{\mathbf{q}} \hbar\omega_{\mathbf{q}} b^\dagger_{\mathbf{q}} b_{\mathbf{q}} + \sum_{\alpha;\mathbf{k},\mathbf{q}} M_{\alpha\alpha}(\mathbf{q}) a^\dagger_{\alpha,\mathbf{k}} a_{\alpha,\mathbf{k}-\mathbf{q}} (b_{\mathbf{q}} + b^\dagger_{-\mathbf{q}}). \quad (1)$$

The creation (annihilation) operators $a^\dagger_{\alpha,\mathbf{k}}$ ($a_{\alpha,\mathbf{k}}$) describe electrons in band $\alpha$ and at wave vector $\mathbf{k}$ in the Brillouin zone. In the excitation term, $\mathbf{v}_{\alpha\beta}(\mathbf{k})$ are the velocity matrix elements, and $\mathbf{A}(t)$ is the vector potential; the $\mathbf{A}^2(t)$ term has been neglected in Eq. (1), since it only introduces a phase shift in the total wave function of the system. We take the vector potential to be

$$\mathbf{A}(t)=[\mathbf{A}_{\omega_0}(t)e^{-i\omega_0 t - i\theta_{\omega_0}} + \mathbf{A}_{2\omega_0}(t)e^{-2i\omega_0 t - i\theta_{2\omega_0}}] + \text{c.c.}, \quad (2)$$

where $\mathbf{A}_{\omega_0}(t)$ and $\mathbf{A}_{2\omega_0}(t)$ are real, slowly varying, envelope functions; the formalism can be also extended to slowly chirped pulses. Intraband scattering is described by the matrix elements $M_{\alpha\alpha}(\mathbf{q})$ for the electron-phonon coupling,[23] without considering phase-dependent prefactors relevant to different bands.[18] In the approximation of a constant LO-phonon energy $\hbar\omega_{\mathbf{q}} \approx \hbar\omega_Q$, they are equal to

$$M^2_{\alpha\alpha}(\mathbf{q}) = M^2(\mathbf{q}) = \frac{M_0^2}{|\mathbf{q}|^2}, \quad M_0^2 = 2\pi e^2 \sqrt{\hbar\omega_Q}\left(\frac{1}{\varepsilon_\infty} - \frac{1}{\varepsilon_0}\right). \quad (3)$$

The $q$-dependence of $M^2_{\alpha\alpha}(\mathbf{q})$ is responsible for the relaxation of the injected carrier momenta. In the numerical calculations below, parameters relevant for GaAs (Ref. 24) are used; $\hbar\omega_Q = 36$ meV, $\varepsilon_0 = 12.5$, and $\varepsilon_\infty = 10.9$.

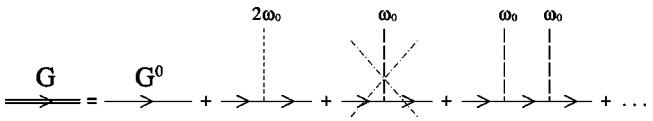


FIG. 2. The diagrammatic expansion of the Green function in the excitation fields. The field self-energy $\mathbf{\Sigma}_f$ results from combination of one- and two-photon diagrams.

## III. DESCRIPTION OF THE TWO-BEAM EXCITATION

We describe the *two-beam coherent control* by nonequilibrium Green functions in a matrix form,[12–16] as defined in Appendix A. The causal function $\mathbf{G}$ in Eq. (A1) satisfies a Dyson equation (integration over $\overline{t_3}, \overline{t_4}$):

$$\mathbf{G}(\mathbf{k};t_1,t_2)=\mathbf{G}^0(\mathbf{k};t_1,t_2) + \mathbf{G}^0(\mathbf{k};t_1,\overline{t_3})\mathbf{\Sigma}(\mathbf{k};\overline{t_3},\overline{t_4})\mathbf{G}(\mathbf{k};\overline{t_4},t_2). \quad (4)$$

Here $\mathbf{G}^0 = G^0_{\alpha\beta}\delta_{\alpha\beta}$ is the free Green function, and $\mathbf{\Sigma}$ is the electron self-energy, which includes contributions from the interaction with the electromagnetic field and the phonons. It can be formally separated into field $\mathbf{\Sigma}_f$ and scattering $\mathbf{\Sigma}_s$ parts, as in one beam excitation, even though here both are functionals of $\mathbf{G}$. While $\mathbf{\Sigma}_s$ has a standard form, determined by the scattering diagrammatics, the field self-energy $\mathbf{\Sigma}_f$ can be constructed by combining the one- and two-photon transitions relevant in this problem. This $\mathbf{\Sigma}_f$ forms an effective external field,[11] whose absolute value gives a natural *expansion parameter*. The injection efficiency can be characterized by the ratio of minimum and maximum values of $\mathbf{\Sigma}_f(\mathbf{k})$ at different $\mathbf{k}$ [see Eq. (6)].

The field self-energy $\mathbf{\Sigma}_f$ can be obtained by expanding $\mathbf{G}$ in the two laser fields. For small excitation energies the real populations are injected only into one conduction ($c$) band and the nearest light- and heavy-hole ($v$) valence bands, while the two-photon part of the carrier injection includes virtual transitions involving all bands.[4] Therefore, the real processes can be described by two-by-two matrix $G_{\alpha\beta}$ ($\alpha,\beta = c,v$). The nonzero off-diagonal elements $\Sigma_{f;cv}$ and $\Sigma_{f;vc}$ for interband driving give the propagators $\Sigma^{r,a}_{f;cv} = \Sigma_{f;cv} = \Sigma^*_{f;vc}$ and the correlation parts $\Sigma^{\langle,\rangle}_{f;\alpha\beta} = 0$.

The first few terms in the diagrammatic expansion of $\mathbf{G}$ in the separate field components from expression (2) are shown in Fig. 2. The terms following include electron-phonon diagrams[25] and diagrams combining the two processes. We use the rotating wave approximation (RWA)[16] throughout, since our focus is on real injected populations. The field with frequency $2\omega_0$ can induce resonant transitions between $c$ and $v$ bands, as shown in Fig. 2 by the first diagram on the right side of $\mathbf{G}^0$. For a field with frequency $\omega_0$, the same diagram is nonresonant (crossed), but that component contributes in second order (and higher even orders), as shown in the next diagram.

In the lowest order, the effective field self-energy $\mathbf{\Sigma}_f$ can be constructed by adding the two diagrams from Fig. 2. In the RWA, it is equal to

$$\Sigma_{f;cv}(\mathbf{k},t_1,t_2) = -\frac{e}{c}\mathbf{v}_{cv}(\mathbf{k})\cdot\mathbf{A}_{2\omega_0}(t_1)e^{-2i\omega_0 t_1 - i\theta_{2\omega_0}}\delta(t_1-t_2) + \frac{e^2}{c^2}\sum_{\alpha}\mathbf{v}_{c\alpha}(\mathbf{k})\cdot\mathbf{A}_{\omega_0}(t_1)G_{\alpha\alpha}(\mathbf{k},t_1-t_2)\mathbf{v}_{\alpha v}(\mathbf{k})\cdot\mathbf{A}_{\omega_0}(t_2)e^{-i\omega_0(t_1+t_2)-i2\theta_{\omega_0}}, \quad (5)$$

where $G_{\alpha\alpha}(\mathbf{k},t_1-t_2)$ corresponds to ''instantaneous'' off-resonant virtual transitions. Dressing of this function is not crucial, unless momentum relaxation is large or higher-order phenomena in the field $\mathbf{A}(t)$ are investigated. In the two-band model adopted here, virtual transitions involving higher bands in the two-photon part from Eq. (5) are neglected ($\alpha = c,v$). Inclusion of these terms[4] would rescale the magnitude of the two-photon amplitude by 10–20 %.

For steady-state excitations, the Dyson equation (4) with the field self-energy $\Sigma_{f;cv}$ from Eq. (5) can be Fourier transformed to the frequency representation.[11] For laser beams polarized in the $x$ direction, this provides the elements

$$\Sigma_{f;cv}(\mathbf{k}) = -\frac{e}{c}v^x_{cv}(\mathbf{k})\left(A^x_{2\omega_0}e^{-i\theta_{2\omega_0}} + \frac{e}{c}(A^x_{\omega_0})^2 e^{-i2\theta_{\omega_0}}\frac{v^x_{cc}(\mathbf{k})-v^x_{vv}(\mathbf{k})}{\hbar\omega_0}\right). \quad (6)$$

In transport equations, the frequency argument of Green functions following $\Sigma_{f;cv}(\mathbf{k})$ are shifted by $2\omega_0$ [see Eq. (B2)]. In the second term of Eq. (6), the free-electron energy $\hbar\omega \approx \varepsilon_c(\mathbf{k})$ is used in the approximate virtual propagators $G^{0,r}_{vv}(\mathbf{k},\omega-\omega_0) \approx -G^{0,r}_{cc}(\mathbf{k},\omega-\omega_0) \approx 1/\hbar\omega_0$, giving opposite signs at $v^x_{cc}(\mathbf{k})$, $v^x_{vv}(\mathbf{k})$. The large bracket in Eq. (6) is an effective excitation field $A_{eff}(\mathbf{k})$ with different amplitudes in the $\pm\mathbf{k}$ directions, since the second term has parity opposite the first term [$v^x_{\alpha\alpha}(\mathbf{k}) = -v^x_{\alpha\alpha}(-\mathbf{k})$]. The direction of $\mathbf{k}$ for which $|A_{eff}(\mathbf{k})|$ is larger can be tuned by adjusting the phases $\theta_{2\omega_0}$ and $\theta_{\omega_0}$, which gives a control over the current directionality. Note that the carrier quasimomentum is conserved during the injection process, while the total *momentum* of carriers injected in each band has the same sign, and it is provided by the lattice.

Quantum interference of the wave-function components coming from the two transition amplitudes can be suppressed if their phases are randomized by scattering. This phase relaxation[26] can be also seen as a decoherence process.[27,28] In a coherent control scheme, with two independent excitation paths, space or time fluctuations either from scattering or external fields could lead to such decoherence, which can be also seen as a kind of inhomogeneous broadening.[29] We defer those issues to future studies.

## IV. KINETIC EQUATIONS

The light-induced current $\mathbf{J}$ is proportional to the momentum imbalance in the nonequilibrium population of carriers. We can conveniently address the description of this imbalance with the *integral* form of the Kadanoff-Baym quantum transport equations.[30,31] This is because the nonequilibrium electron correlation functions $\mathbf{G}^<$ and $\mathbf{G}^>$ (populations) in Eq. (A2) in the zeroth iteration give the field-induced current, which is iteratively dressed by scattering.

The equation for $\mathbf{G}^<$ ($\mathbf{G}^>$) has the following form:

$$\mathbf{G}^<(\mathbf{k},t_1,t_2) = \mathbf{G}^r(\mathbf{k};t_1,\overline{t_3})\mathbf{\Sigma}^<_s(\mathbf{k};\overline{t_3},\overline{t_4})\mathbf{G}^a(\mathbf{k};\overline{t_4},t_2) = \sum_{l=0}^{\infty}\frac{1}{l!}\mathbf{G}^<_l(\mathbf{k},t_1,t_2). \quad (7)$$

Here we neglect the term associated with initial distributions that decays in the presence of interactions,[32] since we assume that inelastic scattering is turned on adiabatically from $t = -\infty$; another approach can be adopted in simplified model situations.[15] The right side of Eq. (7), which includes both injection and scattering, is expanded into contributions $\mathbf{G}^<_l$ in $l$th powers of the field self-energy $\mathbf{\Sigma}_f$, to obtain equations for different order coherent control phenomena. A similar expansion was used by Schäfer and Treusch[12] in a different optical excitation problem.

To close the equations for $\mathbf{G}^<$ and $\mathbf{G}^>$ in Eq. (7), expressions for the nonequilibrium scattering self-energy parts $\mathbf{\Sigma}^<_s$ and $\mathbf{\Sigma}^>_s$ are also needed. We use them in the self-consistent Born approximation[25]

$$\mathbf{\Sigma}^<_s(\mathbf{k},t_1,t_2) = \mathbf{M}(\overline{\mathbf{q}})\mathbf{G}^<(\mathbf{k}-\overline{\mathbf{q}},t_1,t_2)\mathrm{D}^<(\overline{\mathbf{q}},t_1,t_2)\mathbf{M}(\overline{\mathbf{q}}). \quad (8)$$

Here $D$ is the standard phonon Green function in equilibrium,[23] and the $\mathbf{M}$'s are the phonon matrix elements, which are nonzero on the band diagonal [see Eq. (3)]. The nonequilibrium propagators $\mathbf{\Sigma}^{r,a}_s$ result from Eq. (8) as in Eqs. (A3) and (A6).

The propagators $\mathbf{G}^r$ and $\mathbf{G}^a$ in Eq. (7) can be expressed in terms of $\mathbf{G}^<$ and $\mathbf{G}^>$ as in Eq. (A3), or they can be formally obtained by inversion of the Dyson equation (4). In the coherent control problem, the poles of the full $\mathbf{G}^r$ give different quasiparticle spectra at $\pm\mathbf{k}$. The equilibrium propagators $\mathbf{G}^r_0$ have nonzero diagonal elements

$$G^r_{0;\alpha\alpha}(\mathbf{k},\omega) = \frac{1}{\hbar\omega - \varepsilon_\alpha(\mathbf{k}) - \Sigma^r_{0;\alpha\alpha,s}(\mathbf{k},\omega)}, \quad (9)$$

related to the equilibrium correlation functions $G^{\langle,\rangle}_{0;\alpha\alpha}$ as in Eq. (A4). The steady-state form of the first two expansion terms in Eq. (7) is found in Appendix B. In the following, the equations in the second-order term are approximated, starting with the one-particle (spectral) part in the scattering self-energy $\Sigma^r_{0;\alpha\alpha,s}$.

### A. Approximations of the scattering self-energy

In metals, the electron self-energy $\Sigma_s^r(\mathbf{k},\omega)$ for scattering with LA phonons depends weakly on the absolute value of the wave vector $k=|\mathbf{k}|$ because of weak scattering close to the Fermi level and the small ratio of phonon and electron velocities. Therefore, the $k$ dependence of $\Sigma_s^r(\mathbf{k},\omega)$ can be effectively neglected in the derivation of generalized transport equations.[33,34] In polar semiconductors, such as GaAs, the energy difference between electron levels related by LO-phonon emission and absorption processes (see Fig. 1) is comparable to their broadening; i.e., the times scales for phonon oscillation and electron relaxation are of the same order.[21] When the level width is projected through the electron spectral function $A_\alpha(\mathbf{k}-\overline{\mathbf{q}},\omega-\overline{\omega})$ on the momenta, different matrix elements $\mathbf{M}(\overline{\mathbf{q}})$ are encountered in each level, which makes the self-energy (8) momentum dependent.

In a first approximation, we simply neglect this dependence, as is done in metals. The self-energy becomes $k$ independent if the element $\mathbf{M}(\overline{\mathbf{q}})$ is kept fixed in the integration over the absolute value of $|\overline{\mathbf{q}}|$. We set $\overline{\mathbf{q}}$ in $\mathbf{M}(\overline{\mathbf{q}})$ equal to the value $\mathbf{k}_{res}^n-\mathbf{k}_{res}^{n\pm1}$ for the difference of the centers for neighbor levels, located for simplicity at the free-electron energies $E_{res}^n=E_{res}^0+n\hbar\omega_Q$. This approximation freezes the scattering rate *within* each level, but preserves the dependence of the matrix element $M(\mathbf{k}_{res}^n-\mathbf{k}_{res}^{n\pm1})$ on the angle between the initial wave vector $\mathbf{k}_{res}^n$ and the final wave vector $\overline{\mathbf{k}}_{res}^{n\pm1}$. The first can be placed on the $x$ axis, $\mathbf{k}_{res}^n=k_{res}^n(1,0,0)$, and the second in the $k^x$-$k^z$ plane, $\overline{\mathbf{k}}_{res}^{n\pm1}=k_{res}^{n\pm1}[\cos(\overline{\phi}),0,\sin(\overline{\phi})]$, where the angle $\overline{\phi}\in(0,\pi)$ operates. The angle of $\overline{\mathbf{k}}_{res}^n$ in the orthogonal $k^y$-$k^z$ plane is $\overline{\theta}\in(0,2\pi)$. We use parabolic bands with effective masses $m_c=0.067m_e$, $m_{lh}=0.082m_e$, and $m_{hh}=0.53m_e$.

With these approximations, and using Eqs. (8), (9), and (A4), the $k$-independent function $\Sigma_{0;cc,s}^{>}$ ($\Sigma_{0;cc,s}^{<}=0$) for the $n$th level can be obtained in the form

$$\Sigma_{0;cc,s}^{>}(n,\omega)=M_0^2\int_0^{\pi}\frac{d\overline{\phi}}{2\pi}\sin(\overline{\phi})\int_0^{\infty}\frac{d\overline{k}}{2\pi}\overline{k}^2\times\left[\frac{A_c(\overline{k},\omega-\omega_Q)}{|\mathbf{k}_{res}^n-\overline{\mathbf{k}}_{res}^{n-1}|^2}[1+n_B(\omega_Q)]+\frac{A_c(\overline{k},\omega+\omega_Q)}{|\mathbf{k}_{res}^n-\overline{\mathbf{k}}_{res}^{n+1}|^2}n_B(\omega_Q)\right];\tag{10}$$

a similar result holds for $\Sigma_{0;vv,s}^{<}$ ($\Sigma_{0;vv,s}^{>}=0$). The integration over $\overline{\theta}$ gives unity, and $n_B(\omega)=1/[\exp(\hbar\omega/kT)-1]$ is the Bose-Einstein distribution. If the scattering parameter $g=(M_0/\hbar\omega_Q)^2$ increases in value ($g>0.1$),[35] the electron levels become broadened and the optical transitions detuned. Then the $\omega$ dependence of $\Sigma_{0;cc,s}^{>}(n,\omega)$ reflects the changing density of states *within* these quasiparticle levels [see the discussion after Eqs. (14)].

### B. Approximations of the transport equations

We also approximate the transport equations for nonequilibrium correlation functions $G_{2;cc}^{<}$ and $G_{2;vv}^{>}$ to second order in $\Sigma_{f;cv}(\mathbf{k})$. In the steady state, they are found in Appendix C:

$$\begin{aligned}G_{2;cc}^{<}(\xi)&=|G_{0;cc}^r(\xi)|^2[2|\Sigma_{f;cv}(\mathbf{k})|^2G_{0;vv}^{<}(\xi-2\xi^0)+M(\overline{\mathbf{q}})^2G_{2;cc}^{<}(\xi-\overline{\xi})D^{<}(\overline{\xi})],\\G_{2;vv}^{>}(\xi)&=|G_{0;vv}^r(\xi)|^2[2|\Sigma_{f;vc}(\mathbf{k})|^2G_{0;cc}^{>}(\xi+2\xi^0)+M(\overline{\mathbf{q}})^2G_{2;vv}^{>}(\xi-\overline{\xi})D^{>}(\overline{\xi})],\end{aligned}\tag{11}$$

where $\xi=(\mathbf{k},\omega)$, $\xi_0=(0,\omega_0)$. The first terms on the right sides describe the optical injection of carriers by interband transitions; the expansion prefactor 2 cancels 1/2! from Eq. (7). The second terms describe the intraband ''injection'' of phonon relaxed carriers with a different energy and momentum. To keep the picture consistent, these equations, representing the two-particle part of the problem, must be approximated in the same way as the self-energy (10) from the one-particle part. In particular, we make the transport vertices $\Sigma_{2;nn,s}^{\langle,\rangle}$ $k$ independent.

Here the $\overline{\theta}$ integration does not equal unity, since the relaxation of electrons out of the $k^x$ axis (nonzero $\phi$) no longer has cylindrical symmetry. Using the notation $\mathbf{k}_{res}^n=k_{res}^n[\cos(\phi),\sin(\phi),0]$ and $\overline{\mathbf{k}}_{res}^{n\pm1}=k_{res}^{n\pm1}[\cos(\overline{\phi}),\sin(\overline{\phi})\sin(\overline{\theta}),\sin(\overline{\phi})\cos(\overline{\theta})]$, and fixing these vectors in the $|\overline{\mathbf{q}}|$ integration as before, we arrive at the transport vertex in the $k$-independent approximation (10):

$$\Sigma_{2;cc,s}^{<}(n,\phi,\omega)=M_0^2\int_0^{\pi}\frac{d\overline{\phi}}{2\pi}\sin(\overline{\phi})\int_0^{2\pi}\frac{d\overline{\theta}}{2\pi}\int_0^{\infty}\frac{d\overline{k}}{2\pi}\overline{k}^2\times\left[\frac{G_{2;cc}^{<}(\overline{k},\overline{\phi},\omega-\omega_Q)}{|\mathbf{k}_{res}^n-\overline{\mathbf{k}}_{res}^{n-1}|^2}n_B(\omega_Q)+\frac{G_{2;cc}^{<}(\overline{k},\overline{\phi},\omega+\omega_Q)}{|\mathbf{k}_{res}^n-\overline{\mathbf{k}}_{res}^{n+1}|^2}[1+n_B(\omega_Q)]\right].\tag{12}$$

In the following, it will be convenient to denote

$$\begin{aligned}G_{cc}^{<}(n,\phi,\omega)&=\int_0^{\infty}\frac{d\overline{k}}{2\pi}\overline{k}^2G_{2;cc}^{<}(\overline{k},\phi,\omega),\\F(n,\phi;n\pm1,\overline{\phi})&=\int_0^{2\pi}\frac{d\overline{\theta}}{2\pi}\frac{1}{|\mathbf{k}_{res}^n-\overline{\mathbf{k}}_{res}^{n\pm1}|^2},\end{aligned}\tag{13}$$

where $F(n,\phi;n\pm1,\overline{\phi})$ can be evaluated analytically with the use of the formula[36]

$$\int_0^x\frac{d\overline{x}}{a+c\sin(\overline{x})}=\arctan\left(\frac{c+a\,\mathrm{tg}(x/2)}{\sqrt{a^2-c^2}}\right)+C.$$

We can take advantage of the fact that expression (12) is $k$ independent, and integrate Eqs. (11) over $k$, as in studies concerning metals.[31,33,34] This allows us to close the first equation in Eq. (11) in terms of $G_{cc}^{<}(n,\phi,\omega)$, since the propagators $|G_{0;cc}^r(\mathbf{k},\omega)|^2$ become integrated independently from the $k$-independent $\Sigma_{2;cc,s}^{<}(n,\phi,\omega)$. At the same level of approximations, the product $|G_{0;cc}^r(\mathbf{k},\omega)|^2$ $G_{0;vv}^{<}(\mathbf{k},\omega-2\omega_0)$ can be integrated over $k$ (see Appendix C).

Substitution of terms (12), (C1), and (C2) into Eqs. (11) gives the quantum kinetic equation for $G_{cc}^{<}$ in the form

$$G^{<}_{cc}(n,\phi,\omega)=\frac{-k^n_{res}}{\hbar^2\,\mathrm{Im}\,\Sigma^r_{cc,s}(n,\omega)}\Bigg(|\Sigma_{f;cv}(\phi)|^2\mathcal{A}(n,\omega)\mu_{cv}\delta_{n0}+\frac{m_c}{2}M_0^2\int_0^{\pi}\frac{d\bar{\phi}}{2\pi}\sin(\bar{\phi})\{F(n,\phi;n-1,\bar{\phi})$$

$$\times G^{<}_{cc}(n-1,\bar{\phi},\omega-\omega_Q)n_B(\omega_Q)+F(n,\phi;n+1,\bar{\phi})G^{<}_{cc}(n+1,\bar{\phi},\omega+\omega_Q)[1+n_B(\omega_Q)]\}\Bigg). \tag{14}$$

Here $\mu_{cv}=m_cm_v/(m_c+m_v)$ is the effective electron-hole mass, and the equation for $G^{>}_{vv}$ has an analogous form.

These quantum kinetic equations describe the two-beam coherent control for a moderately large scattering. In Eqs. (14), the broadening of the effective spectral function $\mathcal{A}(n,\omega)$, further modified by the $\omega$-dependent $\mathrm{Im}\,\Sigma^r_{0;cc,s}(n,\omega)$, describes the effect of the electron-photon interaction on the carrier generation. Consequently, the transport vertex with populations $G^{<}_{cc}(n\pm1,\bar{\phi},\omega\pm\omega_Q)$ is also broadened, and further modified by $\mathrm{Im}\,\Sigma^r_{0;cc,s}(n,\omega)$. These $\omega$-dependent changes in the transport equations represent *quasiparticle corrections*, which change the relaxation rates,[37] and in transient situations have the character of memory effects. They reflect time-dependent quasiparticle formation, observed in recent one-beam excitation experiments.[20,21] Two-beam coherent control could allow the observation of these phenomena in the induced current.[36]

### C. Boltzmann equation

For weak scattering, the $\omega$ dependence of the self-energy in Eq. (10) can be neglected by using the Markov approximation $\Sigma^{>}_{cc,s}(n,\omega=E^n_{res}/\hbar)$. In this situation we can also use $A_c\approx A^0_c$, which leads to $\Sigma^{>}_{cc,s}$ in the *non*-self-consistent Born form. Then the $k$ integral in Eq. (10) is

$$\int_0^{\infty}\frac{d\bar{k}}{2\pi}\bar{k}^2A_c(\bar{k},E^n_{res}/\hbar\pm\omega_Q)\approx\frac{1}{2}\left(\frac{2m_c}{\hbar^2}\right)^{3/2}\sqrt{E^{n\pm1}_{res}}. \tag{15}$$

The propagators $\Sigma^{r,a}_{0;\alpha\alpha,s}$ can be constructed from $\Sigma^{>}_{0;\alpha\alpha,s}$ as in Eq. (A6).

If the self-energy in Eq. (15) is applied in Eq. (14), then during their integration over $\omega$ the prefactor splits from the rest of the terms and the effective spectral function $\mathcal{A}$ integrates to 1. As a result, we obtain the steady-state integral Boltzmann equation[30] (IBE) for the two-beam optical excitation,

$$f_{cc}(n,\phi)=\frac{2k^n_{res}\tau_o(n)}{\hbar^3}\Bigg(|\Sigma_{f;cv}(\phi)|^2\mu_{cv}\ \ \delta_{n0}+\frac{m_c}{2}M_0^2\int_0^{\pi}\frac{d\bar{\phi}}{2\pi}\sin(\bar{\phi})\{F(n,\phi;n-1,\bar{\phi})f_{cc}(n-1,\bar{\phi})n_B(\omega_Q)$$

$$+F(n,\phi;n+1,\bar{\phi})f_{cc}(n+1,\bar{\phi})[1+n_B(\omega_Q)]\}\Bigg), \tag{16}$$

where the distribution function is

$$f_{cc}(n,\phi)=\int\frac{d\hbar\omega}{2\pi}G^{<}_{cc}(n,\phi,\omega), \tag{17}$$

and $\tau_o(n)=-\hbar/2\,\mathrm{Im}\,\Sigma^r_{cc,s}(n)$ is the particle relaxation time. The relaxation of electron momenta is described by the local transport (momentum relaxation) time[38] $\tau_p\approx3\tau_o$, resulting from $\tau_o(n)$ by inclusion of the vertex correction terms in Eq. (16).[31] To obtain a physically consistent solution of Eq. (16), it is necessary to add the radiative transfer of carriers between the bands. The induced current is not sensitive to the form of this additional term, since mostly levels with small $n$ are affected, where the total momentum of carriers is already very small due to relaxation.

We can similarly derive a time-dependent IBE, necessary for studies of pulsed excitations. It can be obtained from Eq. (7), using approximations analogous to the steady-state case in the time domain,[30] or by a logical generalization of Eq. (16). Its form is as follows:

$$f_{cc}(n,\phi,T)=\frac{2k^n_{res}}{\hbar^3}\int_0^T dT'e^{-(T-T')/\tau_o(n)}\Bigg(|\Sigma_{f;cv}(\phi,T')|^2\mu_{cv}\delta_{n0}+\frac{m_c}{2}M_0^2\int_0^{\pi}\frac{d\bar{\phi}}{2\pi}\sin(\bar{\phi})\{F(n,\phi;n-1,\bar{\phi})$$

$$\times f_{cc}(n-1,\bar{\phi},T')n_B(\omega_Q)+F(n,\phi;n+1,\bar{\phi})f_{cc}(n+1,\bar{\phi},T')[1+n_B(\omega_Q)]\}\Bigg), \tag{18}$$

and it coincides with the steady-state equation (16) for long excitation pulses. Here we use Eqs. (17) and (18) to present the main features in the injection and relaxation of the hot electron population with nonzero average momentum, even though the conditions of weak scattering are not fully satisfied in GaAs.

### D. Induced current density

The solutions of Eqs. (16)–(18) can be used to calculate the optically induced current density **J**. The injection (scattering) term contributes to **J** from the level $n=0$ $(n\neq 0)$. The total current density is formed by the electron and hole parts $\mathbf{J}=\mathbf{J}_{cc}+\mathbf{J}_{vv}$, resulting from the individual bands. For laser beams polarized in the $x$ direction, the current density $J^x_{cc}$ is

$$J^x_{cc}=2e\int\frac{d^3\mathbf{k}}{(2\pi)^3}\int\frac{d\hbar\omega}{2\pi}v^x_{cc}(\mathbf{k})G^<_{cc}(\mathbf{k},\omega)$$

$$\approx\frac{e}{2}\sum_n v_{cc}(k^n_{res})\int_0^\pi\frac{d\phi}{2\pi}\sin(2\phi)f_{cc}(n,\phi), \quad (19)$$

and $J^x_{vv}$ is analogous. In the second expression, we have used $G^<_{cc}\approx f_{cc}/2!$, and $\sin(2\phi)/2$ combines the $\phi$ dependence of the momentum integral $[\sin(\phi)]$ and the $x$ component of the velocity $[\cos(\phi)]$.

In the generation term $f_{cc}(n=0,\phi)$, the mixed part from the squared field self-energy $|\Sigma_{f;cv}(\phi,T)|^2$ contributes to **J**. In steady state it is equal to

$$|\Sigma_{f;cv}(\phi)|^2_{mix}=\frac{2e^3}{c^3}A^x_{2\omega_0}(A^x_{\omega_0})^2\cos(\theta_{2\omega_0}-2\theta_{\omega_0})$$

$$\times|v^x_{cv}(\phi)|^2\frac{v^x_{cc}(\phi)-v^x_{vv}(\phi)}{\hbar\omega_0}, \quad (20)$$

where all the velocities are taken at $k^0_{res}$. The approximate cosine dependence of the intraband matrix elements $v^x_{cc,vv}(\phi)\approx\pm\cos(\phi)$ builds an *imbalance* in the generation of carriers with opposite momenta. The direction of the net current density **J** is controlled by the phases $\theta_{2\omega_0}$ and $\theta_{\omega_0}$.

The angular dependence of the generated population is also determined by the interband velocity elements $v^x_{cv}(\phi)$. We use their approximate *ab initio* values for GaAs, calculated in the absence of spin-orbit interaction, and consider the lowest conduction band, one light-hole band, and two degenerate heavy-hole bands. The square of the interband velocity element $|v^x_{cv}(\phi)|^2$ summed over the two hh bands is approximately $\theta$ independent, as is the value $|v^x_{cv}(\phi)|^2$ for the single light hole band (indicated by our notation). In the parabolic approximation these two then have the forms

$$|v^x_{cv;light}(\phi)|^2\approx v_l^2\cos^2(\phi), \quad |v^x_{cv;heavy}(\phi)|^2\approx v_h^2\sin^2(\phi), \quad (21)$$

where $v_l$ and $v_h$ are constant for a given light energy. Therefore, the conduction-band photogenerated electron distribution in the Brillouin zone has a maximum along (perpendicular to) the polarization direction for generation from lh (hh) band, which is distorted by the mixed term (20). This symmetry has already been recognized in one-photon excitation,[39] where a mixture of the light- and heavy-hole bands close to the $\Gamma$ point was considered. In Sec. V we show that the momentum (current) relaxation has a different character for these two cases. In Appendix D the carrier generation rates obtained here are compared with those found earlier from a Fermi's golden rule calculation.[4]

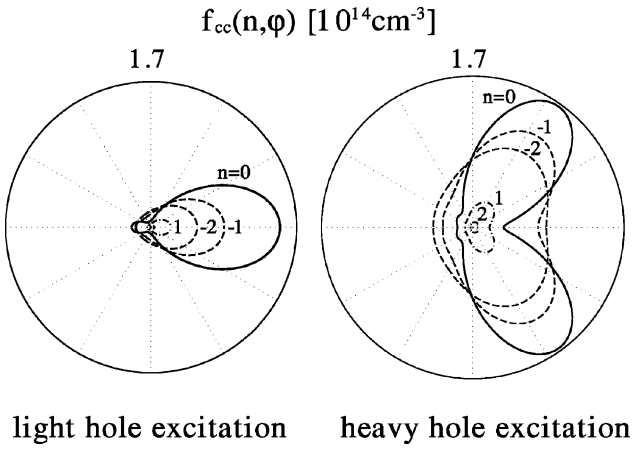


FIG. 3. The steady-state electron distribution in the conduction band, $f_{cc}(n,\phi)$, for lh/hh excitation at $T=300$ K. The full line is for level $n=0$, and dashed (dash-dotted) lines correspond to negative (positive) $n$.

## V. NUMERICAL RESULTS AND DISCUSSIONS

Here we solve Eqs. (16) and (18) and calculate the carrier distribution in the individual levels and the related currents. Results for only the conduction band are presented, since the valence band has similar distributions and contributes less to the total current. Generation of radiation in the THz region by these transient currents is also briefly described.

### A. Electron distribution

We take the energy gap to be $E_g=1.5$ eV, and consider excitation at $2\hbar\omega_0=2.1$ eV. At this energy, the *ab initio* results for $v_l$ and $v_h$ in Eq. (21) are very close to the intraband speed $v_{cc}(k)=\hbar k/m_c$ in the parabolic approximation. Therefore, we approximate them at the excitation point $k^0_{res}$ by the value $v_{cc}(k^0_{res})\approx 1.7$ nm/fs. For the intensities at $2\omega_0$ and $\omega_0$ we take the experimentally realistic values[6] of $I_{2\omega_0}=10$ kW/cm$^2$ and $I_{\omega_0}=100$ MW/cm$^2$, respectively.

In Fig. 3 we present the quasi-steady-state electron distribution in the conduction band, as calculated from Eq. (16). In the left (right) caption we show the results for excitation from the lh (hh) bands. The full line corresponds to the excitation level $n=0$, dashed (dash-dotted) lines are for levels with the one- and two-phonon emission $n=-1$ and $-2$, (absorption, $n=+1$ and $+2$). The temperature is $T=300$ K, so that the phonon absorption is relatively high, and consequently the distributions are nonzero for all angles $\phi$. The photogenerated electron distributions for the lh and hh excitations have a nonzero mean momentum, but their forms are very different from the Fermi sea in metals, when shifted by a dc electric field.[17] Since the two distributions are

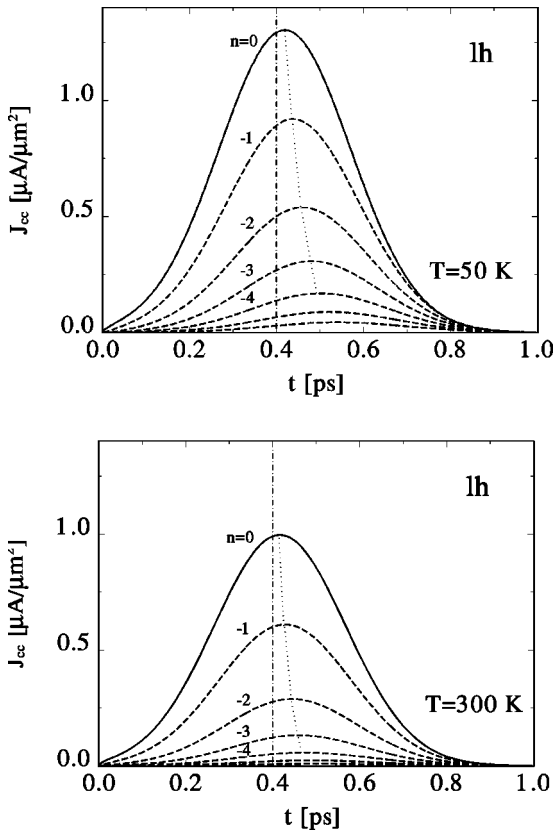


FIG. 4. The current densities $J_{cc}$ for lh excitation at $T=50$ K (upper diagram) and $T=300$ K (lower diagram). The solid line is for $n=0$, and dashed lines correspond to negative $n$. Relaxation at higher temperatures is faster, which gives lower saturated values of the current. The thin vertical dot-dashed line shows the center of the light pulse. The peaks of the individual contributions, shown by the thin dotted line, are shifted with respect to the line.

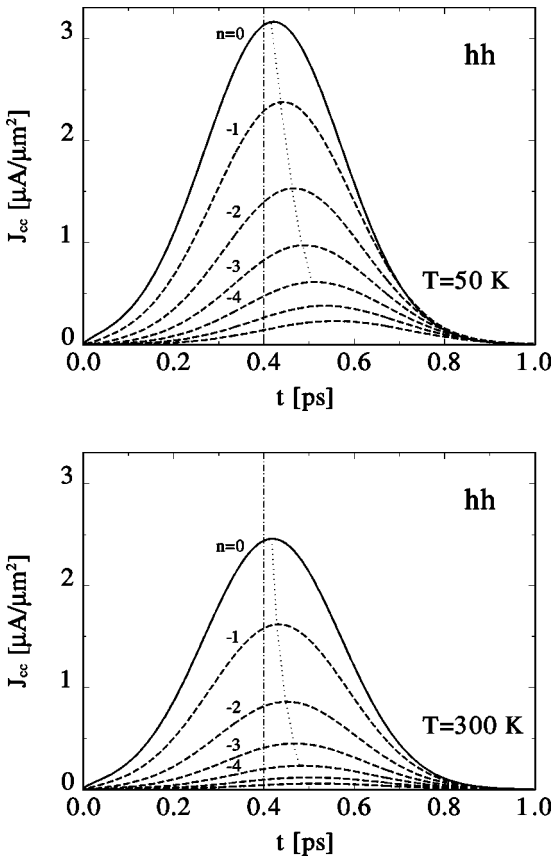


FIG. 5. The same as in Fig. 4 but for the hh excitation. At both temperatures, the relaxation of current is slower than in Fig. 4 and the peaks are more shifted.

also qualitatively different one from another, they have different momentum relaxation times $\tau_p$.

The different shapes of the shifted distributions (along and perpendicular to the $x$ axis for the lh/hh excitation) are determined by the elements $v^x_{cv;light}(\phi)$, $v^x_{cv;heavy}(\phi)$. The relaxation of the $k_x$ component of the wave vector $\mathbf{k}$ has a 2D-like character for electrons generated from lh excitation, since $k_x$ is decreased by scattering in any $\phi$-direction. This relaxation is slower for hh excitation than for lh excitation, since in the hh case the momentum relaxes in a one-dimensional-like form; i.e., $k_x$ relaxes because there is more available phase space for scattering in the direction toward $\phi=90°$ than away from it, while scattering in the $\theta$ direction does not lead to relaxation of $k_x$. The large available phase space for hh excitation also increases the total injected current in this case. Since the distributions for the two excitations are complementary, their sum resembles the change in distribution that would characterize a metal in a dc bias. Relaxation of anisotropy in distributions with zero mean momentum was recently also studied in the presence of carrier-carrier scattering.[40,37]

### B. Photoinduced current

Next from Eqs. (18) and (19) we calculate the time dependent current densities for a pulse excitation. Fields $A_{2\omega_0}(t)$ and $A_{\omega_0}(t)$, with peak intensities as before, are assumed to lead to an effective field $A_{eff}$ with a Gaussian envelope function $e^{-(t-t_0)^2/2\sigma_E^2}$, $t_0=400$ fs, and $\sigma_E=150$ fs. This is typical of experimental conditions, because the pulse $A_{2\omega_0}(t)$ is usually produced from $A_{\omega_0}(t)$ by second-harmonic generation in a doubling crystal, leading to a pulse width of $A_{2\omega_0}(t)$ that is half that of $A_{\omega_0}(t)$.

In Fig. 4 we show the current densities $J_{cc}(n)$ from the individual levels for the lh excitation. In the upper diagram the solution at the low temperature $T=50$ K shows a relatively large shift of maxima for the lower levels, plotted by the thin dotted line, with respect to the center of the laser pulse, represented by the vertical thin dot-dashed line. In the lower diagram we show the corresponding results for $T=300$ K. Here the values are smaller and the relaxation is faster, due to stimulated phonon processes. In Fig. 5 the same is presented for the hh excitation. Here the current contributions are several times larger and they suffer a smaller decrease as we move to levels with smaller $n$. These levels are also more shifted, especially at the lower temperature $T=50$ K. For the assumed Gaussian pulse, it is possible to observe a very small overshoot in the relaxation tail of the current, i.e., levels with smaller $n$ give larger current than those with larger $n$. These effects illustrate the slower momentum relaxation of electrons excited from the hh band.

In Fig. 6 the total current density from the conduction band $J_{cc}$ is shown for lh excitation. The saturation and relaxation time is $\tau_{lh}\approx 70\ (50)$ fs for $T=50\ (300)$ K, which

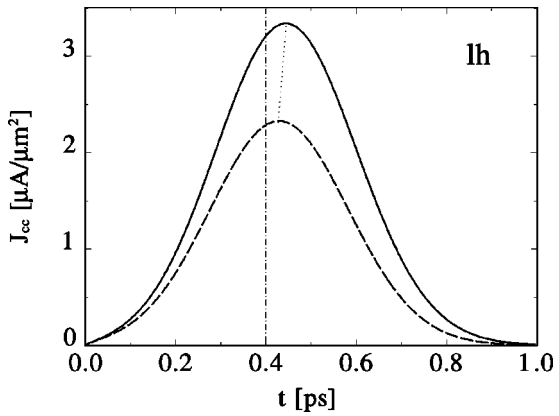


FIG. 6. The total current density $J_{cc}$ for the lh excitation. The solid (dashed) line corresponds to the temperature $T=50$ (300) K.

becomes reflected in the different shifts of these two solutions with respect to the light pulse (vertical dot-dashed line). As in the previous pictures, the peak value for the current at $T=50$ K is larger than that at $T=300$ K. Figure 7 shows the results for $J_{cc}$ in the presence of hh excitation. Here the relaxation times $\tau_{\mathrm{hh}}$ are slightly larger than for the lh excitation at both temperatures, due to the symmetry of the distribution, and the current densities are about three times larger.

In Fig. 8 the steady-state current density $J_{cc}$ is shown as a function of temperature. The solid (dashed) line corresponds to the hh (lh) excitation. At low temperatures the current densities saturate due to spontaneous phonon emission processes. At high temperatures they decrease, because stimulated phonon processes shorten the momentum relaxation time.

### C. Generation of THz radiation

Current pulses in the range of tens of femtoseconds generate electromagnetic radiation in the THz region, originating from the fact that electrons are accelerated during the injection and relaxation. The field typically varies as the derivative of the current density $\mathbf{E}_{emiss}(t)\approx\dot{\mathbf{J}}(t)$. Here we are concerned with the THz radiation generated by the injected currents, and not that generated by displacement currents that persist even at sub-band-gap excitation.[41]

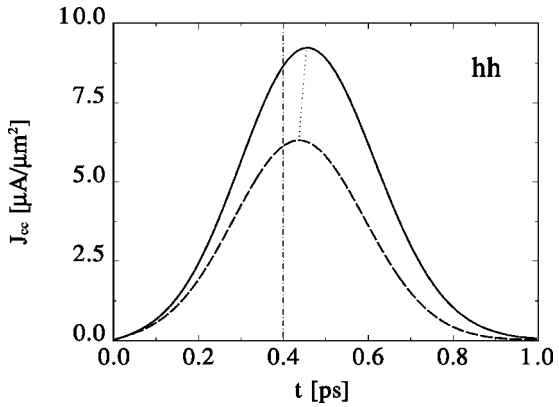


FIG. 7. The total current density $J_{cc}$ for the hh excitation. The saturation and relaxation rates are longer than that found for lh excitation, and the peaks are more shifted.

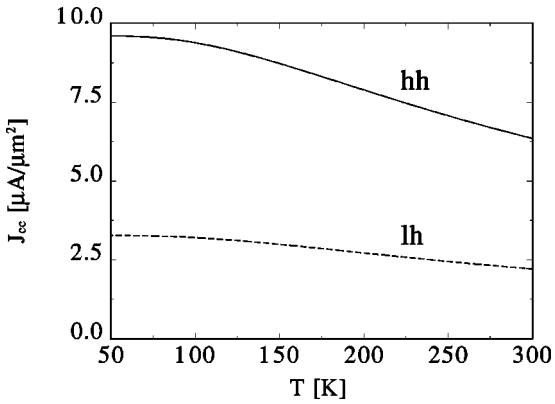


FIG. 8. The steady-state current density $J_{cc}$ as a function of temperature. The solid (dashed) line corresponds to the excitation from heavy (light) holes. Both decay with temperature at appropriate momentum relaxation times.

In Fig. 9 we present the derivative $\dot{J}_{cc}(t)$ for the real hh excitation in our system at the temperature $T=300$ K. We take fields $A_{2\omega_0}(t)$ and $A_{\omega_0}(t)$ with the same peak intensities used above, but given by a Gaussian envelope function with $t_0=150$ fs and $\sigma_E=20$ fs. This short excitation leads to a large asymmetry of $\dot{J}_{cc}(t)$; the sharp increase is produced by the pulse and the slow decay is due to relaxation by phonons. In the inset we show the normalized absolute values of the Fourier components for $\dot{J}_{cc}(t)$. The full (dashed) line corresponds to $\sigma_E=20$ fs ($\sigma_E=100$ fs); both give two peaks symmetric around $\omega_{rad}=0$. If the pulse length is comparable to or longer than the momentum relaxation time $\tau_p$, as in the case of $\sigma_E=100$ fs, the field envelope functions determine the low frequency spectrum. For shorter pulses, as in the case of $\sigma_E=20$ fs, higher-frequency components of the spectrum appear, and at the long-wavelength limit the spectrum is mostly determined by the relaxation of electrons on LO phonons. The THz radiation could reflect nonclassical phenomena in the current, related to polaron formation.[21,36]

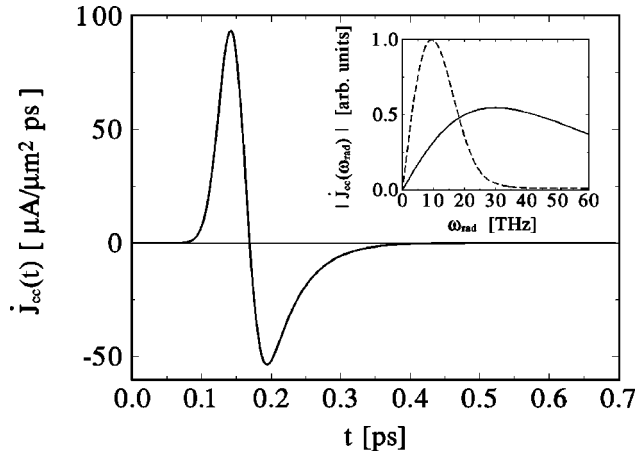


FIG. 9. The derivative $\dot{J}_{cc}(t)$ for hh excitation by two beam pulses of a Gaussian envelope of a width $\sigma_E=20$ fs and at a temperature $T=300$ K. In the inset the spectrum of this derivative is shown. The full (dashed) line corresponds to the pulse width $\sigma_E=20$ fs ($\sigma_E=100$ fs).

## VI. CONCLUSION

We have theoretically investigated the two-laser-beam injection of dc current in bulk semiconductors. This *quantum interference injection* and the carrier relaxation was described by nonequilibrium Green functions. The transition amplitudes for the one- and two-photon transitions at $2\omega_0$ and $\omega_0$ add coherently and form an effective field $A_{eff}(\mathbf{k})$, which generates carriers with different rates at wave vectors $\pm\mathbf{k}$ and produces a dc current. In our diagrammatic approximation, inelastic scattering by LO phonons does not alter this simultaneous two-beam injection, but it is active in redistribution of the carrier's momenta and the current relaxation.

We have derived quantum kinetic equations, in the second order in the field self-energy $\Sigma_{f;cv}(\mathbf{k})$ or equivalently $A_{eff}(\mathbf{k})$. Here the equations have been further simplified to the Boltzmann limit, and applied in steady-state and pulse excitations of GaAs in the presence of LO-phonon scattering. Different electron distributions are photogenerated in the conduction band for excitation from light- and heavy-hole bands. At all temperatures, the total induced current is stronger and it relaxes slower for hh excitation than for lh excitation. Generation of THz radiation by the injected current is also briefly discussed.

It can be expected that other excitation configurations for lasers beams, or materials with a noncentrosymmetric lattice structure, will open further possibilities for direct current injection, with new potential applications.[42] Recently, transport of atoms in carbon nanotubes by the two-beam coherent control was suggested.[43]

## ACKNOWLEDGMENTS

The authors would like to thank A. Shkrebtii for providing *ab initio* matrix elements. We are also grateful H. M. van Driel and D. Côté for helpful discussions. The financial support of this work was provided by Photonics Research Ontario.

## APPENDIX A

We use electron Green functions in a matrix form. In real times and on the quasimomentum diagonal, the causal functions are defined by[16,23,25]

$$G^t_{\alpha\beta}(\mathbf{k},t_1,t_2)=-\frac{i}{\hbar}\langle Ta_{\alpha,\mathbf{k}}(t_1)a^\dagger_{\beta,\mathbf{k}}(t_2)\rangle,\quad \alpha,\beta=c,v, \tag{A1}$$

and the temperature and boson functions can be introduced analogously. The correlation functions $G^>_{\alpha\beta}$ and $G^<_{\alpha\beta}$ are related to $G^t_{\alpha\beta}$ as follows:

$$\begin{aligned} iG^t_{\alpha\beta}(\mathbf{k},t_1,t_2)&=G^>_{\alpha\beta}(\mathbf{k},t_1,t_2)=\langle a_{\alpha,\mathbf{k}}(t_1)a^\dagger_{\beta,\mathbf{k}}(t_2)\rangle/\hbar,\quad t_1>t_2,\\ -i\ \ G^t_{\alpha\beta}(\mathbf{k},t_1,t_2)&=G^<_{\alpha\beta}(\mathbf{k},t_1,t_2)=\langle a^\dagger_{\beta,\mathbf{k}}(t_2)a_{\alpha,\mathbf{k}}(t_1)\rangle/\hbar,\quad t_1<t_2. \end{aligned} \tag{A2}$$

The retarded and advanced propagators $G^{r,a}_{\alpha\beta}$ are defined by

$$\begin{aligned} G^{r,a}_{\alpha\beta}(\mathbf{k},t_1,t_2)=\mp i\,\theta(\pm t_1\mp t_2)[&G^>_{\alpha\beta}(\mathbf{k},t_1,t_2)\\ &+G^<_{\alpha\beta}(\mathbf{k},t_1,t_2)], \end{aligned} \tag{A3}$$

where the $\theta$ function is $\theta(t)=0$ and 1 as $t<0$ and $>0$.

In the steady state the Green functions depend only on the difference of time coordinates $G(\mathbf{k},t=t_1-t_2)$. Then the intraband correlation functions can be expressed after a Fourier transform over $t$ as [11]

$$\begin{aligned} G^<_{\alpha\alpha}(\mathbf{k},\omega)&=n_F(\omega)A_{\alpha\alpha}(\mathbf{k},\omega),\\ G^>_{\alpha\alpha}(\mathbf{k},\omega)&=[1-n_F(\omega)]A_{\alpha\alpha}(\mathbf{k},\omega), \end{aligned} \tag{A4}$$

where in equilibrium $n_F$ is the Fermi-Dirac distribution $n_F(\omega)=1/[\exp(\hbar\omega/kT)+1]$, and the spectral function is defined by the equilibrium correlators

$$A_{\alpha\alpha}(\mathbf{k},\omega)=-2\ \mathrm{Im}\,G^r_{\alpha\alpha}(\mathbf{k},\omega)=G^>_{\alpha\alpha}(\mathbf{k},\omega)+G^<_{\alpha\alpha}(\mathbf{k},\omega). \tag{A5}$$

This relates back to the propagator through the Hilbert transform

$$G^{r,a}_{\alpha\alpha}(\mathbf{k},\omega)=\int_{-\infty}^{\infty}\frac{d\overline{\omega}}{2\pi}\frac{A_{\alpha\alpha}(\mathbf{k},\overline{\omega})}{\omega-\overline{\omega}\pm i\delta}. \tag{A6}$$

## APPENDIX B

In this appendix we consider steady-state current injection and perform a term by term linearization of Eqs. (7) in terms of $\mathbf{\Sigma}_f$.[31] This gives the first-order equation

$$\begin{aligned} \mathbf{G}^<_1=\mathbf{G}^r_0\mathbf{\Sigma}_f\mathbf{G}^<_0+\mathbf{G}^<_0\mathbf{\Sigma}_f\mathbf{G}^a_0+\mathbf{G}^r_0\mathbf{\Sigma}^r_{1s}\mathbf{G}^<_0\\ +\mathbf{G}^<_0\mathbf{\Sigma}^a_{1s}\mathbf{G}^a_0+\mathbf{G}^r_0\mathbf{\Sigma}^<_{1s}\mathbf{G}^a_0, \end{aligned} \tag{B1}$$

where the common arguments $\xi=(\mathbf{k},\omega)$ are not written. In Eq. (B1), the arguments in the $\mathbf{G}_0$ elements that follow $\Sigma_{f(1s);cv}$ and $\Sigma_{f(1s);vc}$ are shifted[31] by $-2\xi^0=(0,-2\omega_0)$ and $2\xi^0$, respectively. We can approximately take $G^<_{0;cc}=G^<_{1;cc}=G^>_{0;vv}=G^>_{1;vv}=0$, while the first-order interband function $G^<_{1;cv}$ fulfills the equation

$$\begin{aligned} G^<_{1;cv}(\xi)=G^r_{0;cc}(\xi)[\Sigma_{f;cv}(\mathbf{k})+\Sigma^r_{1s;cv}(\xi)]G^<_{0;vv}(\xi-2\xi^0)\\ +G^r_{0;cc}(\xi)\Sigma^<_{1s;cv}(\xi)G^a_{0;vv}(\xi-2\xi^0), \end{aligned} \tag{B2}$$

and the expressions for $G^<_{1;vc}$, $G^>_{1;cv}$, and $G^>_{1;vc}$ are analogous. Equation (B2) describes the electron-hole density and the related polarization.[13,44] In the absence of interband scattering, expression (8) gives $\Sigma^<_{1s;cv}(\mathbf{k},\omega)=M_{cc}(\overline{\mathbf{q}})G^<_{1;cv}(\mathbf{k}-\overline{\mathbf{q}},\omega-\overline{\omega})\mathrm{D}^<(\overline{\mathbf{q}},\overline{\omega})M_{vv}(\overline{\mathbf{q}})$. For steady-state excitation, the two Green functions for conduction and valence bands in

each of the vertex correction terms in Eq. (B2), with $\Sigma^{<}_{1;cv}$, cannot both be in resonance, if the energy $\hbar\omega$ is out of the light excited region (phonon emission and absorption). Therefore, these vertex correction terms should be less important in the steady state.

The term $\mathbf{G}^{<}_{2}$ results from expanding $\mathbf{G}$ in Eq. (7) to second order in $\mathbf{\Sigma}_f$:

$$\begin{aligned}\mathbf{G}^{<}_{2}=&2\mathbf{G}^{r}_{0}(\mathbf{\Sigma}^{r}_{f}+\mathbf{\Sigma}^{r}_{1s})\mathbf{G}^{<}_{0}(\mathbf{\Sigma}^{a}_{f}+\mathbf{\Sigma}^{a}_{1s})\mathbf{G}^{a}_{0}+2\mathbf{G}^{r}_{0}(\mathbf{\Sigma}^{r}_{f}+\mathbf{\Sigma}^{r}_{1s})\\&\times\mathbf{G}^{r}_{0}\mathbf{\Sigma}^{<}_{1s}\mathbf{G}^{a}_{0}+2\mathbf{G}^{r}_{0}\mathbf{\Sigma}^{<}_{1s}\mathbf{G}^{a}_{0}(\mathbf{\Sigma}^{a}_{f}+\mathbf{\Sigma}^{a}_{1s})\mathbf{G}^{a}_{0}\\&+2[\mathbf{G}^{r}_{0}(\mathbf{\Sigma}^{r}_{f}+\mathbf{\Sigma}^{r}_{1s})]^{2}\mathbf{G}^{<}_{0}+2\mathbf{G}^{<}_{0}[(\mathbf{\Sigma}^{a}_{f}+\mathbf{\Sigma}^{a}_{1s})\mathbf{G}^{a}_{0}]^{2}\\&+\mathbf{G}^{r}_{0}\mathbf{\Sigma}^{r}_{2s}\mathbf{G}^{<}_{0}+\mathbf{G}^{<}_{0}\mathbf{\Sigma}^{a}_{2s}\mathbf{G}^{a}_{0}+\mathbf{G}^{r}_{0}\mathbf{\Sigma}^{<}_{2s}\mathbf{G}^{a}_{0}.\end{aligned}\tag{B3}$$

The band diagonal elements here describe the injected intraband population. If all terms associated with $\Sigma_{1s}$ are neglected, as discussed above, then Eq. (B3) can be solved independently from Eq. (B1). This gives our starting set of kinetic equations (11). It is worth noting that other terms can contribute to the current. They result from the mixed correlation function $G^{<}_{ij}$, perturbed to a second order in the external field, and give a *shift* current, studied in our next work.[45]

## APPENDIX C

Let us approximate Eq. (11), and start with the $k$ integration in the square of propagators.[31,33] We use the substitution $E=\hbar^2k^2/2m_c$, along with the fact that the approximated self-energy $\Sigma^{r}_{cc;s}(n,\omega)$ is no longer a function of $E$. Then the $E$ integration can be performed in the complex plane [the closed path around the pole $E=\hbar\omega-\Sigma^{r}_{cc;s}(n,\omega)$], with the approximate result[31]

$$\int_0^\infty\frac{dk}{2\pi}k^2|G^{r}_{0;cc}(\mathbf{k},\omega)|^2\approx\frac{-k^n_{res}}{\hbar^2\,\mathrm{Im}\,\Sigma^{r}_{cc,s}(n,\omega)}\,\frac{m_c}{2}.\tag{C1}$$

Here the $E$ integration is approximated by prolongation to $-\infty$, and the square root, resulting from the change of $k$ variable, is taken at the free pole $\hbar\omega=\hbar^2(k^n_{res})^2/2m_c$. More general results for the integral can be also obtained.

The $k$ integral in the excitation (first) term on the right side in Eq. (11) can be done similarly. It is necessary to resolve the spectral function in the valence band from the correlator $G^{<}_{0;vv}=A_{0;vv}$ [$n_F=1$; see Eq. (A4)] into a difference of two propagators $A_{0;vv}=G^{>}_{0;vv}+G^{<}_{0;vv}=i\hbar(G^{r}_{0;vv}-G^{a}_{0;vv})$ [see Eq. (A3)]. These propagators in Eq. (9) are multiplied by $|G^{r}_{0;cc}|^2$. These terms produce two integrals, done as in Eq. (C1), which can be collected to the following form:

$$\int_0^\infty\frac{dk}{2\pi}k^2|G^{r}_{0;cc}(\mathbf{k},\omega)|^2G^{<}_{0;vv}(\mathbf{k},\omega-2\omega_0)\approx\frac{-k^n_{res}\mathcal{A}(n,\omega)\,\delta_{n0}}{2\hbar^2\,\mathrm{Im}\,\Sigma^{r}_{cc,s}(n,\omega)}\,\frac{m_cm_v}{m_c+m_v},$$

$$\mathcal{A}(n,\omega)=-2\frac{\frac{m_c}{m_c+m_v}\mathrm{Im}\,\Sigma^{r}_{cc,s}(n,\omega)+\frac{m_v}{m_c+m_v}\mathrm{Im}\,\Sigma^{r}_{vv,s}(n,\omega)}{(\hbar\omega-\Delta)^2+\left(\frac{m_c}{m_c+m_v}\mathrm{Im}\,\Sigma^{r}_{cc,s}(n,\omega)+\frac{m_v}{m_c+m_v}\mathrm{Im}\,\Sigma^{r}_{vv,s}(n,\omega)\right)^2}.\tag{C2}$$

$$\Delta=\frac{m_c}{m_c+m_v}\mathrm{Re}\,\Sigma^{r}_{cc,s}(n,\omega)+\frac{m_v}{m_c+m_v}[2\hbar\omega_0-E_{gap}+\mathrm{Re}\,\Sigma^{r}_{vv,s}(n,\omega)].$$

Here the particular mass prefactor in $\Delta$ corresponds to the choice of the value $\hbar\omega=0$ at the bottom of the conduction band, but the results are independent of this choice. It is good to stress that the above approximations of the transport equations (11) are consistent with those implied in the $k$-dependent $\Sigma^{>}_{0;cc,s}(n,\omega)$.

## APPENDIX D

Here we compare the generation term from the IBE in Eq. (16) with an analogous term obtained by the Fermi's golden rule.[4] To this end it is more direct to use the differential version of the transport equation[11] for $G^{<}_{cc}$. It has a generation term, in the adiabatic approximation and second order in $\Sigma_{f;cv}$, of the form [Eq. (14.18) from Ref. 16 and Eq. (B2) in this work]

$$\left(\frac{\partial G^{<}_{cc}(\mathbf{k},\omega,T)}{\partial T}\right)_{gen}=\frac{1}{\hbar}|\Sigma_{f;cv}(\mathbf{k})|^2A_{0;cc}(\mathbf{k},\omega)\times A_{0;vv}(\mathbf{k},\omega-2\omega_0).\tag{D1}$$

This expression is equal to the generation term in the steady state $G^{<}_{2;cc}(\mathbf{k},\omega)$ from Eq. (11) multiplied by 1/2! and $-2\ \mathrm{Im}\,\Sigma^{r}_{cc,s}(\mathbf{k},\omega)/\hbar$. Integration of Eq. (D1) over $\mathbf{k}$ and $\omega$, using approximations in the text, yields the first (generation) term in Eq. (18), differentiated over time $T$ at $T=0$. This equivalence of the generation terms in the integral and differential versions of the transport equations allows us to compare the earlier results[4] with expression (D1), instead of Eq. (18).

The time derivative, at $T=0$, of the generation part for the current density in the conduction band is (prefactor 2 for spins)

$$\left(\frac{\partial J^x_{cc}(T)}{\partial T}\right)_{T=0} = 2e\int\frac{d\hbar\omega}{2\pi}\int\frac{d^3k}{(2\pi)^3}v^x_{cc}(\mathbf{k}) \times\left(\frac{\partial G^<_{cc}(\mathbf{k},\omega,T)}{\partial T}\right)_{gen} \approx 2e\int\frac{d^3k}{(2\pi)^3}\frac{v^x_{cc}(\mathbf{k})|\Sigma_{f;cv}(\mathbf{k})|^2}{\hbar^2} \times 2\pi\delta[\omega_{cv}(\mathbf{k})-2\omega_0], \quad \text{(D2)}$$

where Eq. (D1) was used, the $\omega$ integration of the free spectral functions was performed, and the factor $\omega_{cv}(\mathbf{k})=\varepsilon_{\mathbf{k}_c}/\hbar - \varepsilon_{\mathbf{k}_c}/\hbar$ was introduced (isotropic bands). The explicit form of the square $|\Sigma_{f;cv}(\mathbf{k})|^2$ from Eq. (6) can be substituted in Eq. (D2). Further, the vector potential must be written in terms of the electric field, and only two parabolic bands considered. Then the different parts of Eq. (D2) agree with the one-photon, two-photon, and interference terms found by Atanasov *et al.*,[4] when their expressions are subjected to the approximations made here.


[1] P. Brumer and M. Shapiro, Chem. Phys. Lett. **126**, 541 (1986); Y. Y. Yin, C. Chen, and D. S. Elliot, Phys. Rev. Lett. **69**, 2353 (1992).

[2] G. Kurizki, M. Shapiro, and P. Brumer, Phys. Rev. B **39**, 3435 (1989).

[3] E. Dupont, P. B. Corkum, H. C. Liu, M. Budanan, and Z. R. Wasilewski, Phys. Rev. Lett. **74**, 3596 (1995).

[4] R. Atanasov, A. Haché, J. L. P. Hughes, H. M. van Driel, and J. E. Sipe, Phys. Rev. Lett. **76**, 1703 (1996).

[5] A. Haché, Y. Kostoulas, J. L. P. Hughes, J. E. Sipe, and H. M. van Driel, Phys. Rev. Lett. **78**, 306 (1997).

[6] A. Haché, J. E. Sipe, and H. M. van Driel, IEEE J. Quantum Electron. **34**, 1144 (1998).

[7] P. Král and J. Mašek, Acta Phys. Pol. A **82**, 697 (1992).

[8] P. C. M. Planken, I. Brener, M. C. Nuss, M. S. C. Luo, and S. L. Chuang, Phys. Rev. B **48**, 4903 (1993).

[9] A. P. Heberle, J. J. Baumberg, and K. Köhler, Phys. Rev. Lett. **75**, 2598 (1995).

[10] W. Pötz, Appl. Phys. Lett. **71**, 395 (1997).

[11] L. P. Kadanoff and G. Baym, *Quantum Statistical Mechanics* (Benjamin, New York, 1962).

[12] W. Schäfer and J. Treusch, Z. Phys. B: Condens. Matter **63**, 407 (1986).

[13] S. Schmitt-Rink, D. S. Chemla, and H. Haug, Phys. Rev. B **37**, 941 (1988).

[14] K. Henneberger and H. Haug, Phys. Rev. B **38**, 9759 (1988).

[15] A. Kalvová and B. Velický, Z. Phys. B: Condens. Matter **94**, 273 (1994).

[16] H. Haug and A.-P. Jauho, *Quantum Kinetics in Transport and Optics of Semiconductors* (Springer, New York, 1996), Vol. 123.

[17] P. Král and J. Sipe, *Proceedings of the 24th International Conference of the Physics of Semiconductors (ICPS24)*, edited by D. Gershoni (World Scientific, Singapore, 1999).

[18] J. H. Collet, Phys. Rev. B **47**, 10 279 (1993).

[19] R. Bhat and J. E. Sipe (unpublished).

[20] A. Leitenstorfer, C. Fűrst, A. Lauberau, W. Kaiser, G. Trănkle, and G. Weiman, Phys. Rev. Lett. **76**, 1545 (1996).

[21] C. Fürst, A. Leitenstorfer, A. Laubereau, and R. Zimmermann, Phys. Rev. Lett. **78**, 3733 (1997).

[22] M. Combescot and R. Combescot, Phys. Rev. B **37**, 8781 (1988).

[23] G. D. Mahan, *Many Particle Physics* (Plenum, New York, 1981).

[24] P. Y. Yu and M. Cardona, in *Fundamentals of Semiconductors*, edited by P. Treiber and C.-D. Bachem (Springer-Verlag, Berlin, 1996).

[25] A. A. Abrikosov, L. P. Gorkov, and I. Y. Dzyaloshinski, *Quantum Field Theoretical Methods in Statistical Physics* (Pergamon Press, New York, 1965).

[26] B. L. Altshuler and A. G. Aronov, *Electron-Electron Interactions in Disordered Systems*, Modern Problems in Condensed Matter Sciences Vol. 10 (North-Holland, Amsterdam, 1985).

[27] A. Stern, Y. Aharonov, and Y. Imry, Phys. Rev. A **41**, 3436 (1990).

[28] Y. Imry, *Introduction to Mesoscopic Physics* (Oxford University Press, Oxford, 1997).

[29] P. Král, F. W. Sheard, and F. F. Ouali, Phys. Rev. B **57**, 15 428 (1998).

[30] A. P. Jauho, Phys. Rev. B **32**, 2248 (1985).

[31] P. Král, Phys. Rev. B **53**, 11 034 (1996).

[32] A. P. Jauho, N. S. Wingreen, and Y. Meir, Phys. Rev. B **50**, 5528 (1994).

[33] R. E. Prange and L. P. Kadanoff, Phys. Rev. **134**, A566 (1964).

[34] T. Holstein, Ann. Phys. (N.Y.) **29**, 410 (1964).

[35] P. Král and A. P. Jauho, Phys. Rev. B **59**, 7656 (1999).

[36] I. S. Gradshteyn and I. M. Ryzhik, in *Tables of Integrals, Series and Products*, 4th ed., edited by A. Jeffrey (Academic, New York, 1965).

[37] R. Binder, H. S. Kŏhler, M. Bonitz, and N. Kwong, Phys. Rev. B **55**, 5110 (1997).

[38] B. K. Ridley, *Quantum Processes in Semiconductors* (Clarendon Press, Oxford, 1993).

[39] B. P. Zakharchenya, D. N. Mirlin, V. I. Perel, and I. I. Reshiha, Usp. Fiz. Nauk. **136**, 459 (1982) [Sov. Phys. Usp. **25**, 143 (1982)].

[40] J. L. Oudar, A. Migus, D. Hulin, G. Grillon, J. Etchepare, and A. Antonetti, Phys. Rev. Lett. **53**, 384 (1984).

[41] B. B. Hu, A. S. Weling, A. V. Kuzhetson, and C. J. Stanton, Phys. Rev. B **49**, 2234 (1994).

[42] N. Laman, A. I. Shkrebtii, J. E. Sipe, and H. M. van Driel, Appl. Phys. Lett. **75**, 2581 (1999).

[43] P. Král and D. Tománek, Phys. Rev. Lett. **82**, 5373 (1999); E. S. Mele, P. Král, and D. Tomanek, Phys. Rev. B (to be published).

[44] R. W. Boyd, *Nonlinear Optics* (Academic, London, 1992).

[45] P. Král, J. E. Sipe, and K. Busch (in preparation).